



Natural occurring radiation dose and radiological risk assessment around Monoun Lake and surrounding localities in the West region of Cameroon

Felix Haman¹ · David Kpeglo Okoh² · Daniel Bongue^{1,3} · Cebastien Joel Guembou Shouop⁴ · Dorine Flore Tiomene¹ · Dieu Souffit Gondji⁵ · Maurice Ndontchueng Moyo^{1,3,4}

Received: 15 August 2023 / Accepted: 27 April 2024 / Published online: 28 May 2024
© The Author(s), under exclusive licence to Springer-Verlag GmbH Germany, part of Springer Nature 2024

Abstract

The main objective of this study was to assess the natural radiation dose and radiological risk around Lake Monoun and some surrounding localities. A total of 28 soil samples were analyzed using gamma-ray spectrometry based on a High-Purity Germanium detector. The activity concentrations of primordial radionuclides (^{226}Ra , ^{232}Th , and ^{40}K) and the corresponding health hazard risks were determined. The average value of air absorbed dose rate and the total excess lifetime cancer risk were found to be 68.32 nGyh^{-1} and 1.86×10^{-3} . These recorded average values were above the world average value reported by UNSCEAR 2000. RESRAD-OFFSITE computer code was used to evaluate the long-term radiological risk from the study area. The RESRAD simulation data of excess cancer risk was above the world limit of 1.45×10^{-3} until 100 years. The obtained results showed insight into public exposure and could be used as baseline data for future investigations.

Keywords Natural radioactivity · Dose · Radiological risk · Monoun Lake · RESRAD-OFFSITE

Introduction

Cameroon hosts a chain of volcanoes known as the Cameroon Line, stretching for about 1800 km (Issa et al. 2014). This line was hit by a natural disaster in August 1984. Significant amounts of carbon dioxide (CO_2) were released from Lake Monoun (LM) in the western part of Cameroon. This resulted in the loss of human and animal life (Ohba et al. 2022; Sigurdsson et al. 1987). LM is a crater lake located

above a magma reservoir about 800–1000 m thick (Mottet 2000). Crater lakes are lakes that form above a volcanic crater (Rouwet et al. 2015), releasing trapped volcanic gases and accumulating at depth for years. Under the effect of a disruptive event, such as an earthquake, or when the gas concentration reaches saturation point, an inversion of the water layers occurs, causing the gas to rise to the surface at an increasing rate (Tassi and Rouwet 2014).

Disruptive events can cause changes in environmental conditions over time, which can affect environmental radioactivity. Following the unfortunate event at the LM, several studies (Issa et al. 2014; Kusakabe 2017; Cui et al. 2022) have been conducted to comprehend the phenomenon and provide a suitable solution. Carbon dioxide detection systems with alarms have been installed, and degassing columns and systems for collecting meteorological and physicochemical data have also been constructed. However, it is important to note that no radio-ecological study has been conducted yet. Additionally, there are numerous anthropogenic activities such as agriculture, fishing, housing, and sand quarrying for building materials that are developing in and around the lake. The radiological risks associated with these activities are currently unknown. Therefore, it is highly likely that the disruptive events leading to the limnic

✉ Cebastien Joel Guembou Shouop
sebastiangouembou@gmail.com

¹ Centre for Atomic Molecular Physics and Quantum Optics (CEPAMOQ), University of Douala, P.O. Box 8085, Douala, Cameroon

² Radiation Protection Institute, Atomic Energy Commission, P.O. Box LG 80, Legon-Accra, Ghana

³ Department of Physics, Faculty of Sciences, University of Douala, P.O. Box 24157, Douala, Cameroon

⁴ National Radiation Protection Agency, P.O. Box 33732, Yaounde, Cameroon

⁵ Research Centre for Nuclear Science and Technology, Institute of Geological and Mining Research (IRGM), P.O. Box 4110, Yaoundé, Cameroon

explosion also affected the environmental radioactivity. This could have resulted in the release of previously stable radioelements such as ^{238}U , ^{232}Th , and ^{40}K from deep underground, where they had been present since the formation of the earth or other geological processes.

These naturally occurring radioactive elements can be a source of pollution with harmful effects on humans and the environment (Idriss et al. 2016). In addition, the subsoil of these localities is rich in materials that originate from volcanic eruptions. These materials are often used as building materials and can be considered responsible for external gamma radiation exposure. According to UNSCEAR 2000, and the study reported by (Kiprotich Langat and Ambusso 2014), ionizing radiation of natural origin accounts for 79% of the population's exposure, that is an average dose of about 2.4 mSv annually. In addition to cosmic and telluric irradiation, this exposure includes the inhalation of radon gas, which is the most important contributor. Concerning telluric irradiation, it is mainly due to primordial radionuclides (^{238}U , ^{232}Th , and ^{40}K) (Faanu et al. 2014), their contribution to radiation exposure accounts for 55.8%, 14%, and 13.8%, respectively. The assessment of radiation exposure is thus performed by evaluating radionuclide concentrations in different matrices and computing radiological parameters.

The present study aims to evaluate the level of natural radioactivity in soil samples collected around the LM and some surrounding localities. To this end, the activity concentrations ^{238}U , ^{232}Th , and ^{40}K were measured by gamma spectrometry using a high-purity germanium (HPGe) detector on a total of 28 soil samples. The exposure and the risks associated were assessed by evaluating radiological hazards such as the hazard index, absorbed dose, annual effective dose, and cancer risk. This assessment requires knowledge of the activity concentrations of the so-called primordial radionuclides (^{238}U , ^{232}Th , and ^{40}K) at an environmental level.

Study area

The study was conducted at Lake Monoun and some surrounding localities located between $5^{\circ} 34' 47.22''$ N and $10^{\circ} 35' 15.554''$ E in the Kouoptamo subdivision of the West Region of Cameroon, 10 km north of the Foubot town in the Bamoun plain. A map of the study area is shown in Fig. 1. Lake Monoun is a crater lake located on the Cameroon Volcanic Line (CVL) within the Oku Volcanic Group. The geology of the area is dominated by the Precambrian basement complex of Ran-African Quaternary volcano sediments (Kamtchueng et al. 2016). The lithological recognition can be found in (Kamtchueng et al. 2016; Kling et al. 2015; Sigurdsson et al. 1987), and it shows that the geological formations of the area consist of lithologically altered

and fractured basement rocks such as gneiss and migmatite intruded by granite and trachyte. Quaternary volcanic activity is characterized by the presence of basaltic lavas and pyroclastic surge deposits. Recent rock formations are reflected by the presence of alluvial deposits composed of sandy and clayey soils. The soils are characterized by high porosity and permeability due to the fractured and weathered properties of the bedrock and overlying pyroclastic and basaltic rocks.

Experimental setup

Sample collection and preparation

Soil samples were collected along Lake Monoun and some surrounding localities. A total of 28 soil samples were collected randomly in the study area. For each sample, a square area of $2\text{ m} \times 2\text{ m}$ was delimited and cleaned up to remove fresh soil deposited due to weathering. Approximately 1–2 kg of soil was collected from a depth of 5–10 cm. A soil mixture sample was taken at each corner and in the centre of the square area. The collected sample was put into a polyethylene plastic bag and marked to avoid contamination and confusion between different samples. They were sent to the laboratory (Research Centre for Nuclear Science and Technology, of the Institute of Geological and Mining Research, Yaoundé, Cameroon) for preparation. After drying at 105°C for up to 24 h in an oven to ensure complete loss of moisture, the samples were crushed and then sieved using a sieve with a mesh diameter of about 2 mm. All the experimental supplies were cleaned after each preparation with distilled water and 95% methyl alcohol to avoid any contamination. The prepared homogenized samples were packed in a plastic bag, labelled again, and sent to the laboratory of the Radiation Protection Institute, Ghana Atomic Energy Commission (RPI/GAEC) for analysis. At the RPI/GAEC laboratory, the samples were dried again in an oven, to remove moisture. The samples were then packed into a previously weighted 225 mL cylindrical containers, sealed, and kept in a laboratory at room temperature for ~4 weeks to allow for equilibrium between radium and radon (Chauhan et al. 2014).

Gamma-ray spectrum analysis

Measurements were performed using a High-resolution gamma spectrometry system with an Extended Range Germanium coaxial detector (Cannera Model GX4018 with carbon-Epoxy window) with a relative efficiency of 40% and an energy resolution of 2.0 keV for gamma-ray energy of 1332 keV of ^{60}Co , installed at the RPI/GAEC. The detector was placed in a 10 cm lead shield lined with copper,

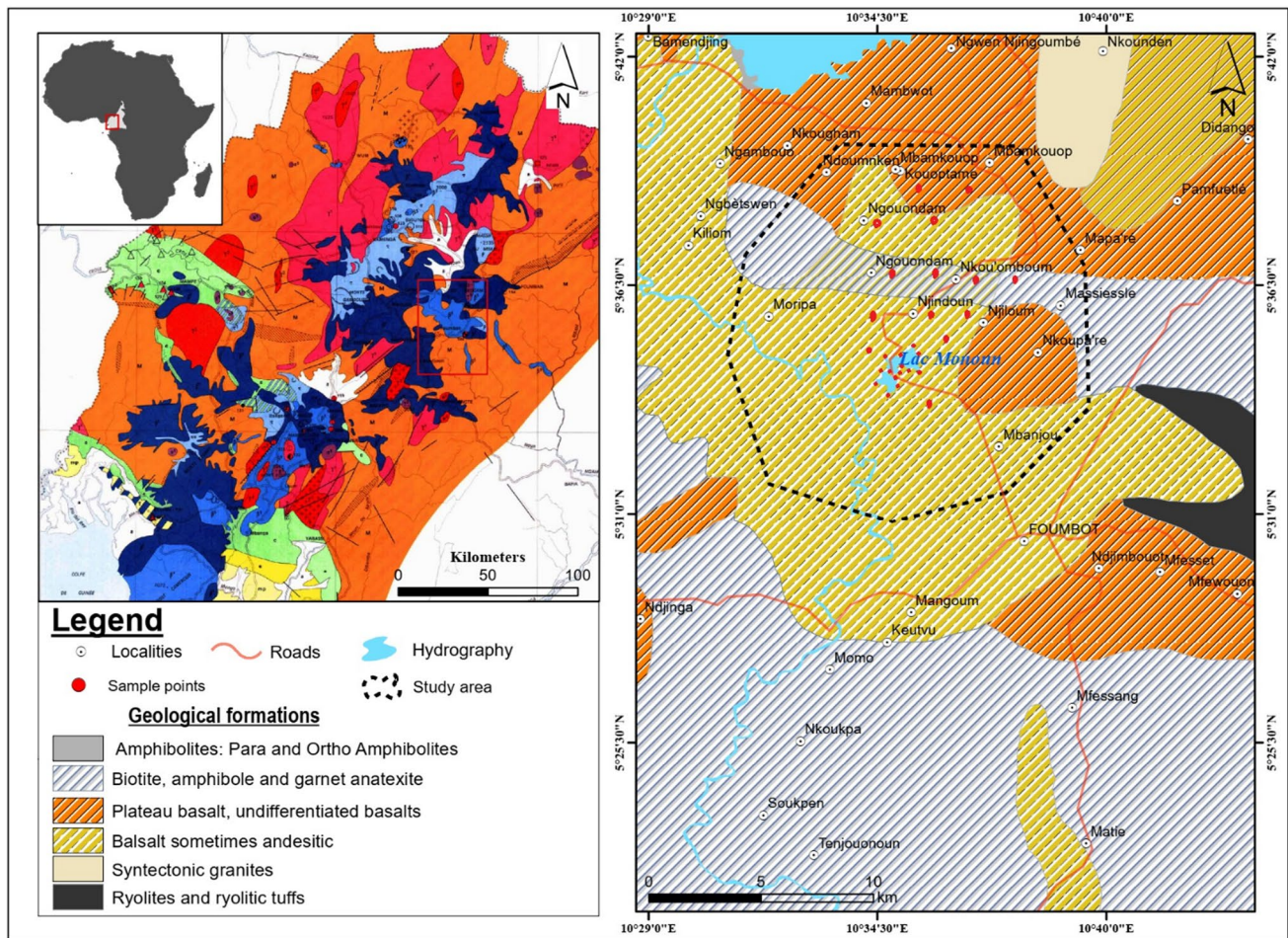


Fig. 1 Map of the study area presenting the sampling points

cadmium, and Plexiglas sheets for background radiation reduction from materials and cosmic rays. The detector was coupled to a Canberra data acquisition system applying Genie-2000 gamma acquisition analysis software (GENIE 2000, Canberra). Before counting gamma radiation in the samples, standard reference materials [IAEA-RGU-1 (U ore), IAEA-RGTh-1 (Th ore), and IAEA-RGK-1 (K ore), with activities of 0.182 kBq, 0.119 kBq, and 0.514 kBq, respectively] having similar densities with the measured soil samples after pulverization, were prepared in similar geometry containers to calibrate the efficiency of the measuring system.

A multi-gamma certified cocktail standard (^{241}Am (3.42 kBq), ^{109}Cd (5.09 kBq), ^{57}Co (0.08 kBq), ^{139}Ce (0.015 kBq), ^{113}Sn (0.024 kBq), ^{85}Sr (0.00081 kBq), ^{137}Cs (2.70 kBq), ^{60}Co (2.49 kBq), and ^{88}Y (0.037 kBq)) in a 1L Marinelli beaker was used for energy calibration of the gamma system. The standard was counted on the detector until the count rate of total absorption could be calculated with a statistical uncertainty of < 5% at a confidence level of

95%. The net counts for each of the full energy events in the spectrum was determined and their corresponding energies used in the determination of the efficiencies.

^{226}Ra , ^{232}Th , and ^{40}K activity concentration analysis.

The prepared samples were submitted to a gamma-ray spectrometer with a coaxial germanium detector (HPGe detector) and counting was performed for 36,000 s (10 h). For the activity concentration estimation, considering a situation of secular equilibrium between ^{238}U , ^{232}Th , and their respective decay daughter products, the following γ -rays photo-peak were used: for ^{226}Ra , the energy lines of ^{214}Bi (609 and 1120 keV) and ^{214}Pb (295 and 352 keV); for ^{232}Th , the energy lines of ^{228}Ac (338 and 911 keV) and ^{208}Tl (583 keV). The ^{40}K was directly determined from its energy line at 1460 keV (Guembou Shouop et al. 2017, 2021).

The environment background was also taken into account by counting an empty sample container for the same counting time as the sample, and substrate to the respective count

rate for each radionuclide in the sample measured to obtain the net count rate under the most prominent photo-peak. The net count rate for each photo peak obtained after subtracting the background was used for activity concentration estimation. The activity concentration of each radionuclide in a specific sample was determined using the following equation:

$$C = \frac{(K_{Sam} - K_{Bac})}{E_{ff} \times P_{\gamma} \times T_C \times M_{Sam}} \pm \sigma \tag{1}$$

$$\sigma^2 = C^2 \left[\left(\frac{\sigma_K}{K} \right)^2 + \left(\frac{\sigma_{E_{ff}}}{E_{ff}} \right)^2 + \left(\frac{\sigma_{P_{\gamma}}}{P_{\gamma}} \right)^2 + \left(\frac{\sigma_{M_{Sam}}}{M_{Sam}} \right)^2 \right] \tag{2}$$

where C is the activity concentration of radionuclide $Bqkg^{-1}$, K_{sam} is the sample net counts, K_{Bac} is the background net counts, E_{ff} is the detector efficiency of photopeak, P_{γ} is the gamma emission probability, T_C is the counting time (second), M_{Sam} is the sample mass (kg), and σ is the activity concentration uncertainty.

The minimum detectable activities (MDA) were calculated from the background spectrum for gamma measurements according to Eq. (3) (Hartwell 1975)

$$MDA = \frac{\left(2.71 + 4.65 \sqrt{K_{Bac} \left(\frac{T_c}{T_{Bac}} \right) + N_C} \right)}{T_c \times E_{ff} \times P_{\gamma}} \tag{3}$$

where K_{Bac} is the background count for the region of interest of each radionuclide, T_C is the sample measurement time, T_{Bac} is the background counting time, N_C is the integral, P_{γ} is the gamma emission probability (gamma yield) of each radionuclide, E_{ff} is the photopeak efficiency for the measured gamma ray energy.

With ~ 200,000 s as normal measuring time in environmental samples, and after applying Eq. (3) to both background and environmental soil sample measurements, levels of MDA were calculated in the gamma system. The calculated MDA for energy lines 295, 351, 609, 1120, 583, 338, 911, and 1460 keV were 5.04, 3.29, 2.82, 7.94, 2.92, 7.73, 4.76, and 23.28 $Bq kg^{-1}$, respectively.

Radiological hazard and risk assessment

Absorbed dose rate in the air (D_{Abs})

The external radiation due to exposure to gamma radiation from radionuclides is expressed as the absorbed dose rate. The knowledge of this parameter is the first step in assessing the radiological risk in a given environment (Alzubaidi et al. 2016). According to UNSCEAR (2000), it is measured at 1 m above the ground surface, to ensure the

uniformity of the radionuclide distribution (Ndontchueng et al. 2014; UNSCEAR 2000). It is obtained by applying the conversion factors ($\alpha = 0.462 \text{ nGyh}^{-1}$ per $Bq kg^{-1}$, $\beta = 0.604 \text{ nGyh}^{-1}$ per $Bq kg^{-1}$, and $\mu = 0.0417 \text{ nGyh}^{-1}$ per $Bq kg^{-1}$) to the activity concentrations of ^{226}Ra (C_{Ra}), ^{232}Th (C_{Th}), and ^{40}K (C_K), respectively. This is given by the following formula (Alzubaidi et al. 2016; UNSCEAR 2000):

$$D_{Abs} = \alpha C_{Ra} + \beta C_{Th} + \mu C_K \tag{4}$$

where: D_{Abs} is the absorbed dose rate to air in $nGyh^{-1}$, and C_{Ra} , C_{Th} , and C_K were the concentrations in $Bqkg^{-1}$ of ^{226}Ra , ^{232}Th , and ^{40}K , respectively.

Annual effective dose rate

The outdoor annual effective dose E_{rate} (outdoor) is given by the following equation (UNSCEAR 2000; Kayakökü and Dođru 2017; Kurnaz et al. 2020):

$$E_{rate}(\text{outdoor}, mSvyr^{-1}) = D_{Abs} \times T \times 0.2 \times 0.7 \times 10^{-6} \tag{5}$$

The health risk of radiation from radionuclides in the environment is assessed in terms of annual effective dose. It is obtained by converting the absorbed dose rate into an effective dose using the dose conversion factor (0.7 SvGy^{-1} , the external occupancy factor (0.2), and the indoor occupancy factor (0.8) (Kurnaz et al. 2020).

Considering the occupancy time and the type of building material (earth material), indoor exposure becomes significant and intrinsically higher than outdoor exposure. Indoor exposure is thus generally considered to be about 40% higher than outdoor exposure (UNSCEAR 2000). As presented in (UNSCEAR 2000) and reported by (Chauhan et al. 2014) the indoor/outdoor ratios vary from 0.60 to 2.3, with a population-weighted value of 1.4 for different countries. Given the above, it is not realistic to use the same dose rate for both indoor and outdoor effective dose calculations. Taking this into account, the indoor annual effective dose can be determined by the following relationship (Chauhan et al. 2014):

$$E_{rate}(\text{indoor}, mSvyr^{-1}) = (D_{Abs} \times 1.4) \times T \times 0.8 \times 0.7 \times 10^{-6} \tag{6}$$

And the total annual effective dose is given by the following equation:

$$E_{rate}(\text{total}, mSvyr^{-1}) = E_{rate}(\text{outdoor}) + E_{rate}(\text{indoor}) \tag{7}$$

where: T ($24 \text{ h} \times 365 \text{ days} = 8760 \text{ h}$) is the number of hours in a year and 0.7 SvGy^{-1} is the coefficient for converting an absorbed dose in the air into an effective dose received by an adult (Ndontchueng et al. 2014).

Effective dose rate (EDR_{organ}) to different body organs and tissues

The effective dose can be delivered to specific organs or tissues from indoor and outdoor air doses and is defined as the amount of radiation dose intake to various body organs and tissues. It's obtained by using the following equation (Darwish et al. 2015):

$$EDR_{organ} (\mu Sv yr^{-1}) = E_{rate} \times CF \quad (8)$$

where CF is the conversion factor of organ dose from air dose and is equal to: 0.82, 0.58, 0.64, 0.69, 0.62, and 0.68 for testes, ovaries, lung, bone marrow, kidneys, and whole body, respectively.

Excess lifetime cancer risk (ELCR)

The stochastic effect of radiation can be assessed by the probability of cancer risk due to exposure to low doses of radiation. It is defined by the ELCR and is expressed by the following relationship (Kurnaz et al. 2020; Turhan et al. 2018):

$$ELCR(\text{outdoor}) = E_{rate}(\text{outdoor}) \times E_L \times RF \quad (9)$$

$$ELCR(\text{indoor}) = E_{rate}(\text{indoor}) \times E_L \times RF \quad (10)$$

$$ELCR(\text{total}) = ELCR(\text{outdoor}) + ELCR(\text{indoor}) \quad (11)$$

where: E_L is the life expectancy for a human being [58.9 years for the Cameroonian population (Gondji et al. 2022)] and RF is the risk factor for stochastic effects produced by low background radiation (0.057 Sv^{-1}).

Annual gonadal dose equivalent

It is generally known that ionizing radiation exposure affects living organisms on both a genetic and somatic level. These outcomes are the main contributors to the development of cancer and numerous tissue damage types. Even though many human body tissues are vulnerable to ionizing radiation, UNSCEAR 2000 states that particular organs, including the gonads, active bone marrow, and bone surface cells, are important (Sivakumar et al. 2014; Darwish et al. 2015; Penabei et al. 2018, 2022; Tiomene et al. 2023). To assess the potential effects of the primordial radiations on these target organs, the annual gonadal dose equivalent (AGDE) was assessed using the following equation (Darwish et al. 2015; Penabei et al. 2022; Sivakumar et al. 2014):

$$AGDE = 3.09C_{Ra} + 4.18C_{Th} + 0.314C_K \quad (12)$$

External and internal hazard index

The estimated radiation dose expected to be delivered externally by soil/sand/rock when used as building materials is given by the external hazard index (H_{ex}) (UNSCEAR 2000). Material is safe when its value is less than 1 (Ndontchueng et al. 2014). Different models are proposed to calculate the external hazard index. Two models were used according to different types of buildings encountered in the study area. It was noted that some houses were built using bricks made of earth building material without window and the door is generally closed the whole day due to the population activity (major are the farmers). Also the presence of standard rooms, build with a door and a window was observed. These two models were the major types encountered in the study area. UNSCEAR (2000) proposed a model for a room with no door and no windows, and the H_{ex} is obtained from the following equation:

$$H_{ex} (\text{no door, no window}) = \frac{C_{Ra}}{370} + \frac{C_{Th}}{259} + \frac{C_K}{4810} \leq 1 \quad (13)$$

Other authors estimated the H_{ex} with the modified model of a room, with door and windows, which will cause ventilation of the room and decrease inhabitant's exposure to radiation, and at the same time decrease the received dose. For this model, the external hazard is given as followed (Darwish et al. 2015):

$$H_{ex} (\text{with door, and window}) = \frac{C_{Ra}}{740} + \frac{C_{Th}}{518} + \frac{C_K}{9620} \leq 1 \quad (14)$$

In addition to the external radiation hazard, radon and its short-lived daughters are also hazardous to the respiratory organs. Internal exposure to ^{222}Rn gas and its progenies is monitored by the internal hazard index (H_{in}). It's given by the following equation (Darwish et al. 2015; Li et al. 2017; Penabei et al. 2022).

$$H_{in} = \frac{C_{Ra}}{185} + \frac{C_{Th}}{259} + \frac{C_K}{4810} \leq 1 \quad (15)$$

Statistical analysis

Statistical analysis is the process of collecting and analysing large amounts of data to discern patterns and trends to convert them into meaningful information. In this work, using the IBM SPSS software package version 23 for Windows, a statistical study of the features of the distribution of the pertinent radiological variables was conducted. The data from the soil samples and the computed radiological

risk parameters were analysed in this study using a basic statistic method and the correlation test.

Basic statistical investigation

A descriptive statistical analysis focuses on creating a basic visual description of the data. The central tendency and fluctuations of the data were described using the arithmetic mean (AM), geometric mean (GM), median (Median), standard deviation, variance, and the interquartile range. The nature of the distribution of natural radionuclides and radiological risk factors was investigated by providing the analysis of the Skewness, the Kurtosis, the histogram, the box plot, the Kolmogorov–Smirnov test, and the Shapiro–Wilk test.

Correlation test

To verify the degree of connection and the relationship between the obtained radiological risk parameters and natural radionuclides a correlation test was performed. According to (Ogundele et al. 2020), in statistics, a correlation coefficient is used as a measure of the relationship between two variables. This coefficient varies between -1 and $+1$. As the correlation coefficient value goes towards 0, the relationship between the two variables will be weaker. The direction of the relationship is indicated by the sign of the coefficient; a $+$ sign indicates a positive relationship and a $-$ sign indicates a negative relationship.

Long-term excess cancer risk analysis using Resrad-OFFSITE computer code

Radioactive elements such as ^{238}U , ^{232}Th , ^{40}K , or ^{222}Rn released from the depth to the surface of the ground during the Lake Monoun limnic eruption can be sources of pollution and contamination of the environment. These radionuclides may be the cause of long-term adverse effects on human health and the environment (Indongo and Mathuthu 2023). Dose and risk assessment for the long term is essential for the management of an environment contaminated by long-lived radioactive elements. The main objective of this assessment is to provide evidence that human health and the environment will be adequately protected in the future.

In this work, for the assessment of the long-term radiological risk, the code RESRAD-OFFSITE version 4.0 was used. The RESRAD-OFFSITE computer code was developed by the Environmental Science Division, Argonne National Laboratory, Department of Energy (DOE), USA to assess the radiation dose and excess cancer risk to an exposed individual when lived or worked in or near primary radionuclide-contaminated site (Hussain et al. 2017; Yu et al. 2009, 2015). With the estimated radioactive concentrations

in the environment, it calculates radiological dose and excess lifetime cancer risk and provides soil clean-up recommendations corresponding to a given dosage limit (Yu et al. 2009).

Different exposure scenarios can be modelled by the Resrad-Offsite code, with 4 main scenarios: rural resident farmer, urban resident, worker, and recreational (Yu et al. 2020). For the modelling in this work, the exposure scenario considered is that of a rural resident farmer. It is assumed that the farmer resides mainly off-site (nearby) and only engages in his daily activities on-site (farming, fishing, grazing, and hunting). It is supposed that 80% of the local produce (vegetables, cereals), meat, milk, and fish products the resident consumes are grown on the site. The rural resident has been exposed to external radiation, both indoors and outdoors. He breathes air contaminated by dust from the re-suspended contaminated soil. The water used for drinking, cooking, and bathing comes from wells located near the site, assuming that they receive the maximum amount of contaminant from the site. The water used for irrigation of the fields comes directly from the lake. The exposure pathways considered in calculating the risk at our site are direct exposure to soil contaminants, inhalation of radioactive dust in suspension, ingestion of plants grown on the site, ingestion of meat and milk from cows, goats, and sheep raised on the site, ingestion of hunting meat from the site, ingestion of fish from the lake, and ingestion of water.

Result and discussion

^{226}Ra , ^{232}Th and ^{40}K activity concentration

This section presents and discusses the activity concentrations of the radionuclides ^{226}Ra , ^{232}Th , and ^{40}K in soil samples in the study area. The activity concentrations of ^{226}Ra ranged from 8.3 ± 0.9 to 127.5 ± 2.3 Bqkg $^{-1}$, with a mean value of 34 Bqkg $^{-1}$. The recorded activity concentrations of ^{232}Th and ^{40}K varied from 9.9 ± 1.9 to 227.2 ± 4.0 and from 61 ± 8 to 909 ± 95 Bqkg $^{-1}$, with mean values of 70 and 252 Bqkg $^{-1}$, respectively. The study results show that some of the primordial radionuclides have a higher average activity concentration compared to their world average value, as defined in UNSCEAR (UNSCEAR 2000). The mean activity concentration value of ^{226}Ra was slightly higher than the world mean value of 32 Bqkg $^{-1}$, while ^{232}Th had a mean activity concentration value that was significantly higher than the world mean value of 45 Bqkg $^{-1}$. The average activity concentration of ^{40}K was found to be lower than the world average value of 420 Bqkg $^{-1}$. As shown in Fig. 2, 43% of the analysed soil samples had ^{226}Ra activity concentrations above the World average, with some cases showing values up to three times higher. Furthermore, 68% of the soil samples had ^{232}Th activity concentrations above the

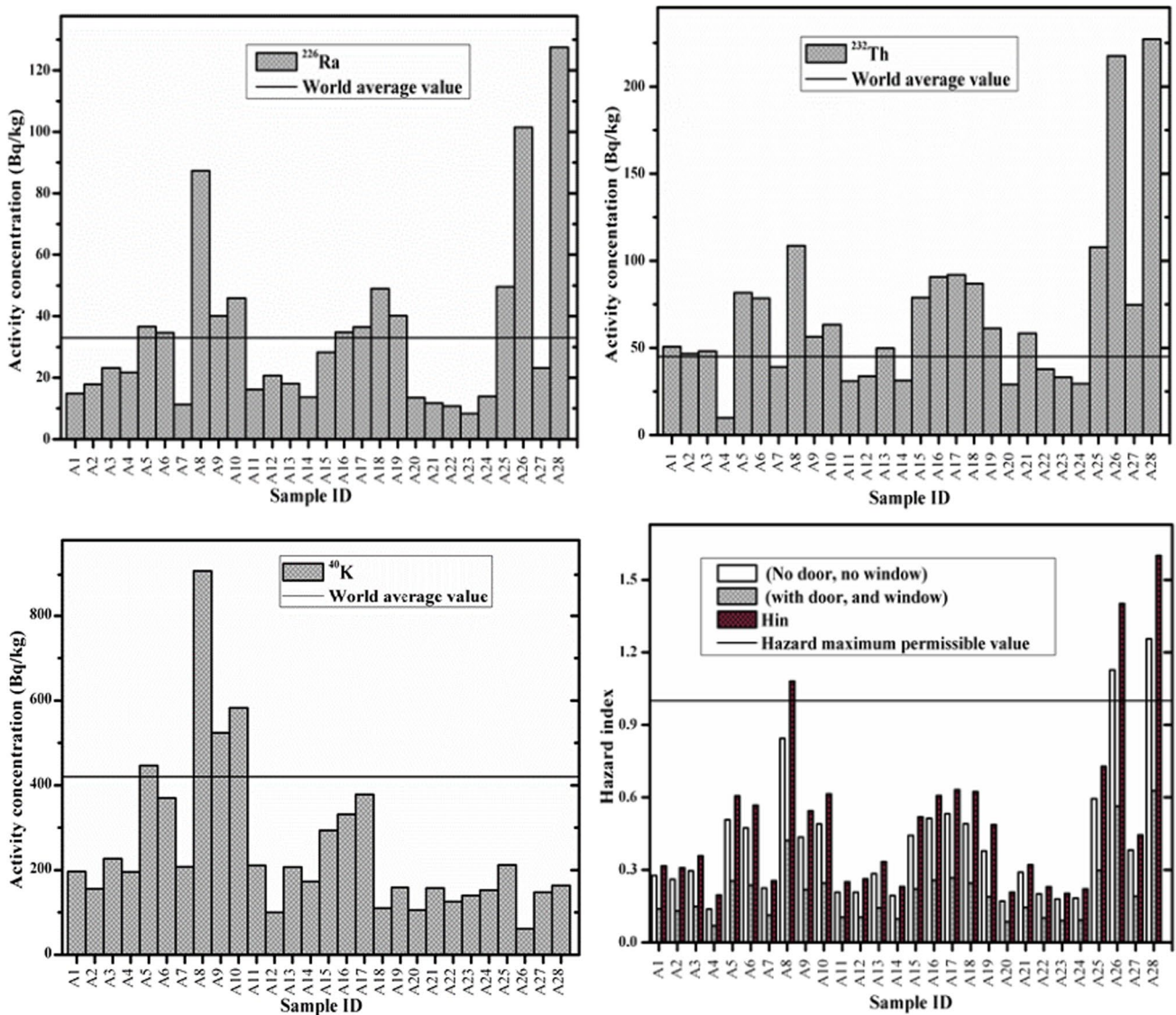


Fig. 2 Distribution of the activity concentrations of primordial radionuclides and the hazard index in the investigated area

global average of 45 Bqkg^{-1} . Regarding ^{40}K , 14% of the soil samples had activity concentrations above the World average. The activity concentrations of ^{232}Th and ^{40}K in some soil samples were 5 and 2 times higher than their respective global averages.

The high radium activity concentration found in some samples is probably caused by the presence of granitic rocks in the geological formation of the area. According to Dabayneh et al. (Dabayneh et al. 2008), granitic rock formations usually have high levels of uranium, which is the precursor to radium. Furthermore, 68% of the soil samples showed a high occurrence of ^{232}Th , which can be explained by their sedimentary origin around the lake, which is generally characterized by high thorium content (Ndontchueng et al. 2014). The elevated levels of ^{40}K in

certain soil samples may be attributed to the presence of rock formations, such as migmatites, which are composed of feldspar and other minerals that are often abundant in potassium (Mekongtso Nguelem et al. 2016). Alternatively, the high activity concentrations in the area may be due to the extensive use of potassium-rich fertilizers in agricultural activities.

Figure 2 displays the distribution of radioactivity concentrations for various radionuclides. The analysis demonstrates the variation of radionuclide activity concentrations between samples, likely due to the heterogeneous distribution of radionuclides in the earth’s crust (Mekongtso Nguelem et al. 2016) and the non-uniform sampling locations.

Additionally, a comparison was conducted between the mean activity concentrations of the radionuclides presented

in this study and those found in other soil investigations in selected areas of Cameroon. The study reported that the average activity concentration values of ^{226}Ra , ^{232}Th , and ^{40}K were higher in the Fongo-Tongo locality, located in western Cameroon (Mekongtso Nguelem et al. 2016), compared to the average activity concentration values of the same radionuclides obtained in the current survey. (Ndjana Nkoulou II et al. 2018) and (Ngachin et al. 2007) reported lower average activity concentration values in their respective studies conducted in the localities of Lolodorf (South, Cameroon) and Buea and Limbe (South-West, Cameroon) compared to the values obtained in this study. These variations in activity concentrations observed from one region to another are likely caused by differences in the geological structures of each site. These structures define the radioactive properties of the soil and describe the deposition and migration processes of the minerals.

Radiological hazard and risk assessment

Materials containing radionuclides can pose a health hazard, with the degree of hazard dependent on the concentration of radionuclides present. To assess the radiological risk associated with the use of this soil, risk parameters and hazard indices can be estimated. Table 1 and Fig. 2 display the radiological health risks in the soil samples. Risk parameters, including air absorbed dose rates (D_{abs}), annual effective doses (E_{rate}), excess lifetime cancer risks (ELCR), annual effective dose equivalents to organs ($\text{ADR}_{\text{organ}}$), annual gonadal dose equivalents (AGDE), and some hazard indices, have been estimated.

The absorbed gamma dose rate in outdoor air (D_{abs}) at a height of 1 m from the ground was calculated using Eq. (4). Table 1 presents the variation of the absorbed dose rate in air as studied. The measured values range from 24.17 to 202.96 nGyh^{-1} , with a mean of 68.32 nGyh^{-1} . The mean absorbed dose rate recorded was higher than the world population-weighted average value of 59 nGyh^{-1} , as defined in UNSCEAR (2000). Some soil samples recorded absorbed dose rate values three times higher than the maximum permissible limit. Furthermore, 50% of the total samples registered an outdoor absorbed dose rate higher than the maximum allowable limit. Therefore, some parts of the investigated area may not be entirely safe for the local population.

Table 2 present the comparison of the air absorbed dose rates data recorded in this study from soil samples with those obtained locally and in other countries. As shown in the Table 2, the absorbed dose rate in air varies from one sampling point to another. This variation is linked to the geological origin and nature of each area (Mekongtso Nguelem et al. 2016).

The study examined the prevalent construction types in the area, where mud bricks were predominantly used as building material. Two types of exposure were considered: outdoor exposure for those working in the open air, and indoor exposure for those living in houses built with mud bricks made from earth material sourced from the study area. Table 1 presents the results of the annual effective dose for outdoor, indoor, and total exposure obtained in this study. The summary of the annual effective dose shows that the outdoor annual effective dose value ranged from 0.03 to 0.25 mSvyr^{-1} , with an average of 0.08 mSvyr^{-1} . The indoor annual effective dose ranged from 0.17 to 1.39 mSvyr^{-1} , with an average of 0.47 mSvyr^{-1} . The total annual effective dose due to external exposure obtained in this study ranged from 0.19 to 1.29 mSvyr^{-1} , with an average of 0.55 mSvyr^{-1} .

In a typical background environment, the average annual effective dose due to external exposure is estimated to be 0.48 mSvyr^{-1} . This is composed of an average of 0.07 mSvyr^{-1} for outdoor exposure and 0.41 mSvyr^{-1} for indoor exposure, according to UNSCEAR (2000). The annual effective dose results for individual countries generally fall within the range of 0.3 to 0.6 mSvyr^{-1} . The average annual effective dose obtained in this study falls within this range. However, some samples showed values that were three times higher than the permitted maximum of 0.48 mSvyr^{-1} . It is crucial to pay special attention to these types of samples as they may pose a radiological hazard to the population.

The excess lifetime cancer risk (ELCR) values indicate the probability of developing cancer for an individual exposed to ionising radiation in a particular area. The ELCR values calculated in this study are presented in Table 1. Outdoor ELCR values range from 0.09×10^{-3} to 0.84×10^{-3} , with an average of 0.28×10^{-3} . Indoor ELCR values range from 0.56×10^{-3} to 4.68×10^{-3} , with an average of 1.58×10^{-3} . The study found that the total ELCR ranges from 0.66×10^{-3} to 5.52×10^{-3} , with an average of 1.86×10^{-3} . The mean value of outdoor excess lifetime cancer risk is slightly lower than the global average of 0.29×10^{-3} . However, the mean value of indoor and total ELCR is higher than their global average value of 1.16×10^{-3} and 1.45×10^{-3} , respectively (James et al. 2020). Approximately 50% of the total soil samples showed indoor and total ELCR values higher than their global average value.

The study found AGDE results ranging from 169.88 to 1395.04 μSvh^{-1} , with an average of 475.53 μSvh^{-1} . This average value exceeds the global average of 300 μSvh^{-1} (Avwiri and Tutumeni 2016). In certain soil samples, the AGDE value was 4.6 times higher than the acceptable limit.

Figure 3 presents the rates of effective dose that can be delivered to specific organs from external exposure. The estimated average $\text{EDR}_{\text{organ}}$ values for testes, ovaries, lungs, bone marrow, kidneys, and whole body were 0.45, 0.32,

Table 1 Distribution of radiological and risk parameters in the study area

Sample ID	D _{rate} (nGy/h)	E _{rate} (mSv/yr)			ELCR (10 ⁻³)			AGDE (μSv/y)
		Outdoor	Indoor	Total	Outdoor	Indoor	Total	
A1	45.60	0.06	0.31	0.37	0.19	1.05	1.24	319.04
A2	42.87	0.05	0.29	0.35	0.18	0.99	1.16	298.71
A3	49.22	0.06	0.34	0.4	0.2	1.13	1.34	343.93
A4	24.17	0.03	0.17	0.2	0.1	0.56	0.66	169.89
A5	84.89	0.10	0.58	0.69	0.35	1.96	2.31	594.93
A6	78.84	0.10	0.54	0.64	0.32	1.82	2.14	551.32
A7	37.49	0.05	0.26	0.3	0.15	0.86	1.02	263.510
A8	143.8	0.18	0.99	1.16	0.59	3.32	3.91	1009.06
A9	74.49	0.09	0.51	0.6	0.31	1.72	2.02	524.49
A10	83.75	0.10	0.58	0.68	0.34	1.93	2.28	589.46
A11	34.95	0.04	0.24	0.28	0.14	0.81	0.95	245.52
A12	34.10	0.042	0.23	0.28	0.14	0.79	0.93	236.36
A13	47.06	0.06	0.32	0.38	0.19	1.09	1.28	329.03
A14	32.38	0.04	0.22	0.26	0.13	0.75	0.88	227.01
A15	72.98	0.09	0.5	0.59	0.3	1.68	1.98	509.47
A16	84.69	0.10	0.58	0.69	0.35	1.95	2.3	590.81
A17	88.21	0.11	0.61	0.71	0.36	2.03	2.4	616.19
A18	79.70	0.10	0.55	0.65	0.33	1.84	2.17	549.13
A19	62.23	0.08	0.43	0.5	0.26	1.43	1.69	430.41
A20	28.17	0.04	0.19	0.23	0.12	0.65	0.77	196.19
A21	47.18	0.06	0.32	0.38	0.19	1.09	1.28	329.24
A22	33.00	0.04	0.23	0.27	0.14	0.76	0.9	230.44
A23	29.72	0.04	0.2	0.24	0.12	0.69	0.81	208.35
A24	30.60	0.04	0.21	0.25	0.13	0.71	0.83	214.18
A25	96.86	0.12	0.67	0.78	0.4	2.23	2.63	670.41
A26	180.88	0.22	1.24	1.46	0.74	4.17	4.92	1242.48
A27	61.99	0.08	0.43	0.5	0.26	1.43	1.68	430.25
A28	202.96	0.25	1.39	1.64	0.84	4.68	5.52	1395.04
Min	24.17	0.03	0.17	0.2	0.10	0.56	0.66	169.89
Max	202.96	0.25	1.39	1.64	0.84	4.68	5.52	1395.04
Mean value	68.32	0.08	0.47	0.55	0.28	1.58	1.86	475.53
World Mean	59	0.07	0.41	0.48	0.29	1.16	1.45	300

Min = Minimum value: refers to the minimum value of the radiological and the risk parameters obtained in the current study

Max = Maximum value: refers to the maximum value of the radiological and the risk parameters obtained in the current study

Mean: refers to the mean value of the radiological and the risk parameters obtained in the current study

Mean World: refers to the mean worldwide value of the radiological and the risk parameters

0.35, 0.38, 0.34, and 0.38 mSvyr⁻¹, respectively. All average values reported in this work are below the international tolerable limits of 1.0 mSvyr⁻¹ (James et al. 2020). The study findings suggest that living in the study area is safe and that there are no immediate radiation effects on specific organs for inhabitants in the locality.

The mean values obtained for the study area regarding the external and internal hazard indexes (refer to Fig. 2) are lower than unity. The hazard index values for a model house with no door and window were slightly higher than unity.

However, when a door and window were added, all values obtained were below unity. This suggests that the entire soil sample can be safely used as a building material for a standard model house with a door and window.

Statistical data analysis

In the current project, basic statistical analysis was used to draw a basic visual description of the data characteristics of all radionuclide parameters. The measured radionuclide data

Table 2 Comparison of air absorbed dose rate with other previous studies for soil samples

Country (study location area)	Air absorbed dose rate (nGyh ⁻¹) Range (mean value)	References
Cameroon (Fongo-Tongo)	96.1–321.2 (188.2)	Mekongtso Nguelem et al. (2016)
Cameroon (Buea and Limbe, south-west region)	27–37 (29)	Ngachin et al. (2007)
Cameroon (Region of Lolodorf)	23.0–47.3 (36.7)	Ndjana Nkoulou II et al. (2018)
Cameroon (Douala-Bassa zone, Littoral region)	90.95–115.77 (98.18)	Ndontchueng et al. (2014)
Turkey (kabarık province)	19–72 (41)	Kurnaz et al. (2020)
Nigeria (Abua/Odual district)	309.5–1226.5 (654.2)	Avwiri and Tutumeni (2016)
Egypt (Nile River)	12.71–38.17 (24.17)	El-Gamal et al. (2007)
Turkey (Van Lake)	10–200 (60)	Kayakökü and Dođru (2017)
Kenya (Lake Nakuru)	48.86–106.8 (71.97)	Kiprotich Langat and Nadir Omar Willis Ambusso (2014)
Malaysia (State of Kedah)	60.71–129 (87.47)	Alzubaidi et al. (2016)
India	239–595 (370)	Mann et al. (2018)
Cameroon (Lake Monoun area)	24.17–202.96 (68.32)	This study

is summarised in Table 3, which shows a positively skewed distribution with an asymmetric tail extending to the right. The data also has a positive kurtosis (> 0), indicating a leptokurtic (sharp) distribution (Yalcin et al. 2020).

To assess the normality of the data, Kolmogorov–Smirnov and Shapiro–Wilk tests were performed (Mishra et al. 2019). The results are shown in Table 4. If $P > 0.05$, the null hypothesis is accepted, indicating that the data are normally distributed. Conversely, if $P < 0.05$, the null hypothesis is rejected, indicating that the distribution is asymmetric. The current study found that all radionuclide parameters had significance values less than 0.05 (Sig. < 0.05), leading to the rejection of the null hypothesis and the assumption that the data are asymmetrically distributed.

The study analysed the distribution frequencies of radiological parameters and presented them using histograms in Figs. 4 and 5. However, the histograms of the obtained radionuclide data indicate some degree of multimodality. This feature of the natural radionuclide in soil demonstrates the complexity of the mineral in the soil sample (Abdullahi et al. 2019).

Figures 4 and 5 show box plots used to assess the normal distribution of activity concentrations and radiological parameters. The radionuclide data in this work indicates that for certain data sets, such as air absorbed dose rate, ²³²Th activity concentration, and ⁴⁰K activity concentration, the box plot closely aligns with the median values, indicating a symmetrical distribution. However, the data set for ²²⁶Ra activity concentrations was not symmetrically distributed. Additionally, many outliers were observed, which could be attributed to measurement variability or experimental error (Abdullahi et al. 2019). In investigations of natural radioactivity, outliers cannot be eliminated simply because they deviate significantly from other samples. Therefore, in

such cases, the data may be assumed to be non-normally distributed.

Prior to conducting a correlation test, we assessed the normality of the data's distributions using the Kolmogorov–Smirnov and Shapiro–Wilk tests. As a result, we used Spearman's rank correlation, and the data obtained is presented in Table 5. The analysis reveals a strong correlation between the concentration of ²²⁶Ra and ²³²Th in the soil samples in our study area. This correlation suggests that high concentrations of ²²⁶Ra are related to high concentrations of ²³²Th. The relationship between the two radioactive series can be attributed to their combined decay in nature (Ravisankar et al. 2014). Furthermore, no strong correlations were observed between the concentrations of ⁴⁰K and the activity concentrations of other primordial radionuclides (²²⁶Ra and ²³²Th). The results indicate that high activity concentrations of ⁴⁰K do not necessarily correspond to high concentrations of other radionuclides in the studied soil samples.

The ranks of the radiological parameters are highly correlated between radiological parameters and the activity concentrations of ²²⁶Ra and ²³²Th, but not with those of ⁴⁰K. An increase in the activity concentrations of ²²⁶Ra and/or ²³²Th would result in an increase in the received dose rate, the annual effective dose, and consequently, the risk of cancer in the area. However, an increase in the concentration of ⁴⁰K is associated with only a slight increase in radiological risks. Therefore, the contribution of ⁴⁰K to external exposure in the studied localities is low.

Long-term radiological effect (excess cancer risk)

The long-term radiological risk assessment in this study takes into account the Cameroonian expectancy lifetime of

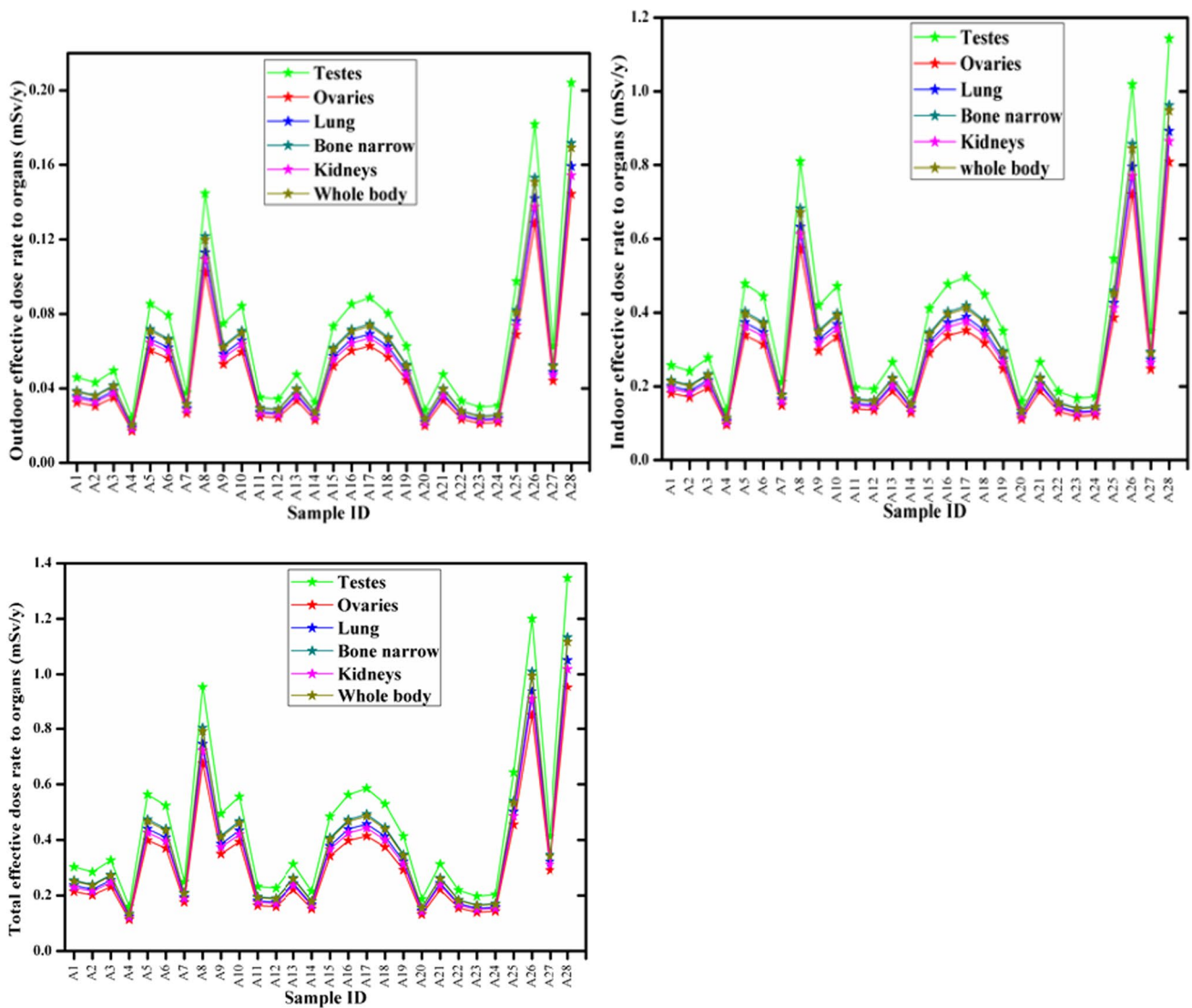


Fig. 3 Distribution of effective dose equivalent rate to different organs or tissues

Table 3 Basic statistical data for activity concentration and radiological risk parameters coefficient

Statistical parameters	Activity concentration (Bqkg ⁻¹)			Radiological risks parameters				
	²²⁶ Ra	²³² Th	⁴⁰ K	D _{abs} (nGyh ⁻¹)	AGDE (μSvh ⁻¹)	H _{in}	H _{ex} (no door, no window)	H _{ex} (with door and window)
Mean	34	70	252	68.32	475.53	0.51	0.41	0.21
Std. Dev	28.6	50.1	182.2	44.53	306.68	0.35	0.27	0.14
Min	8.3	9.9	61.4	24.17	169.88	0.2	0.14	0.07
25th%	14.1	34.8	148.8	34.32	238.65	0.25	0.21	0.1
Median	23	57	196	56	387	0.4	0.34	0.17
75th%	40.1	85.6	322.2	84.46	590.47	0.61	0.5	0.25
Max	127.5	227.2	908.8	202.96	1395.04	1.6	1.26	0.63
Variance	818.1	2511.0	33,189.4	1983.01	94,053.14	0.12	0.08	0.02
Skewness	2.02	2.1	2.15	1.73	1.7	1.88	1.8	1.8
Kurtosis	4.09	4.9	5.45	3.01	2.85	3.59	3.36	3.36

Table 4 Normality test of all recorded data

	Kolmogorov-Smirnov ^a			Shapiro–Wilk		
	Statistic	Df	Sig.	Statistic	Df	Sig.
²²⁶ Ra	0.199	28	0.06	0.758	28	0.000
²³² Th	0.186	28	0.014	0.770	28	0.000
⁴⁰ K	0.269	28	0.00	0.768	28	0.000
D _{ab}	0.185	28	0.015	0.804	28	0.000
E _{rate}	0.185	28	0.015	0.804	28	0.000
ELCR	0.185	28	0.015	0.804	28	0.000
AGDE	0.180	28	0.020	0.808	28	0.000
H _{in}	0.217	28	0.002	0.777	28	0.000
H _{ex} (no door, no window)	0.189	28	0.011	0.798	28	0.000
H _{ex} (with door, and window)	0.189	28	0.011	0.798	28	0.000

^aLilliefors Significance Correction

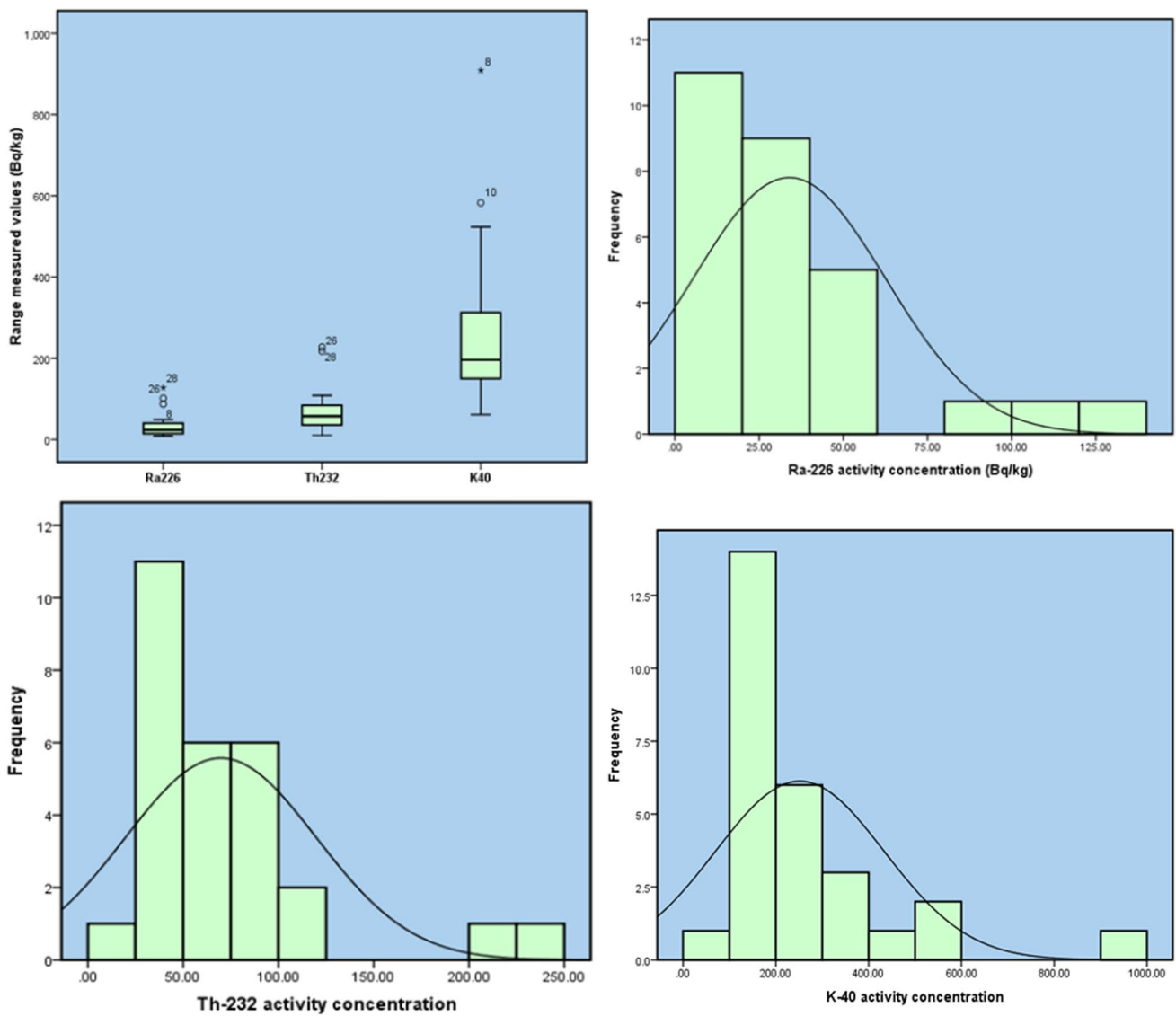


Fig. 4 Frequency distribution and variability of the activity concentrations

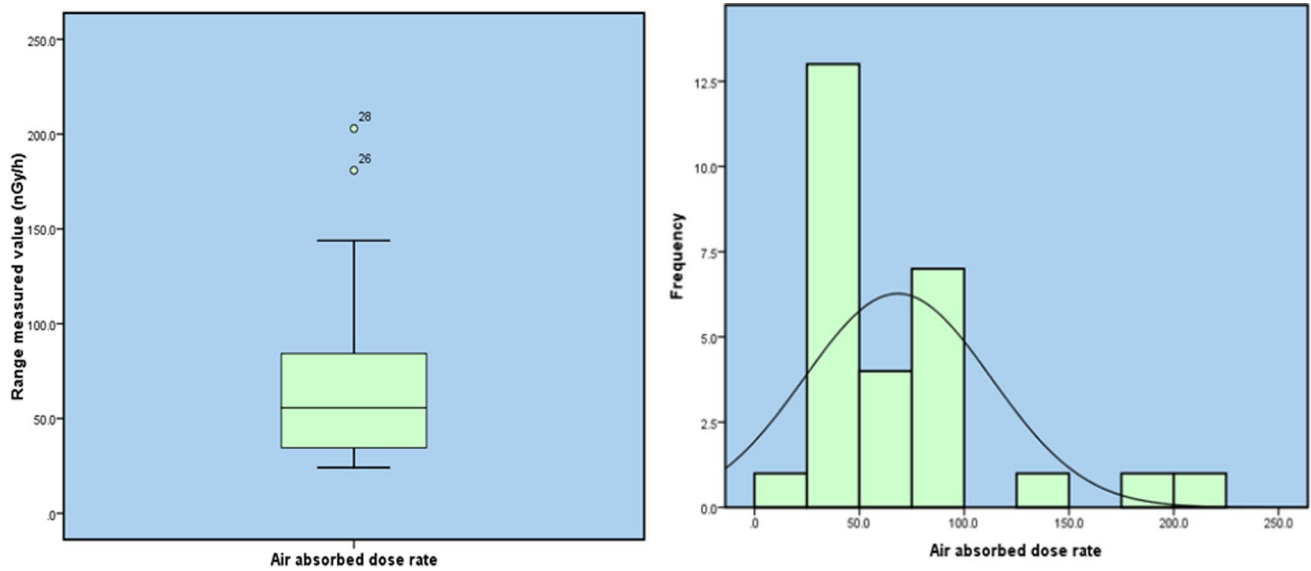


Fig. 5 Frequency distribution and variability of air absorbed dose rate

Table 5 Spearman rank correlation test between radioactive variables for soil samples analysis

	²²⁶ Ra	²³² Th	⁴⁰ K	D _{ab}	E _{rate}	ELCR	AGDE	RLI	H _{in}	H _{ex} (1)	H _{ex} (2)
²²⁶ Ra	1										
²³² Th	0.81**	1									
⁴⁰ K	0.36	0.34	1								
D _{ab875} **	0.88**	0.97**	0.45*	1							
E _{rate}	0.88**	0.97**	0.45*	1.00**	1						
ELCR	0.88**	0.97**	0.45*	1.00**	1.00**	1					
AGDE	0.87**	0.96**	0.47*	0.99**	0.99**	0.99**	1				
RLI	0.87**	0.97**	0.45*	0.99**	0.99**	0.99**	0.99**	1			
H _{in}	0.89**	0.96**	0.42*	0.99**	0.99**	0.99**	0.98**	0.99**	1		
H _{ex} (1)	0.86**	0.97**	0.44*	0.99**	0.99**	0.99**	0.99**	0.99**	0.99**	1	
H _{ex} (2)	0.86**	0.97**	0.44*	0.99**	0.99**	0.99**	0.99**	0.99**	0.99**	1.00**	1

**Correlation is significant at the 0.01 level (2-tailed)

*Correlation is significant at the 0.05 level (2-tailed)

58.9 years (Gondji et al. 2022), and the dose library used is that of ICRP 107. The details of the input data are presented in Table 6.

The simulation results of excess cancer risk for each radionuclide and total risk during 100 years of exposure using RESRAD-OFFSITE computer code version 4.0 are presented in Table 7 and Fig. 6.

The RESRAD modelled cancer morbidity risk shows a maximum total risk of 2.78×10^{-3} at year 0, which slightly decreases to 1.85×10^{-3} over 100 years. The main contributor to the total excess cancer risk in the first 15 years was ⁴⁰K, with ²³²Th becoming the most significant contributor thereafter. The cancer morbidity risk recorded over 100 years was higher than the world average cancer risk of 0.29×10^{-3} , as defined by UNSCEAR 2000, and still exceeds the world

limit value of 1.45×10^{-3} (James et al. 2020; Indongo and Mathuthu 2023).

The analysis shows that ⁴⁰K significantly contributes to the total cancer risk for the first 15 years of exposure across all summed exposure pathways. This contribution decreases slightly over time before dropping significantly after 100 years. The continuing decrease in the risk associated with ⁴⁰K may be attributed to soil erosion and leaching by rainwater. Exposure to ²³²Th increases the risk of cancer morbidity. The risk rises from 8.65×10^{-4} in the first year to a maximum of 1.04×10^{-3} at 30 years, and then stabilises at 1.04×10^{-3} until 100 years. This increase in risk is attributed to the contribution of the ingrowth progenies of ²²⁸Ra and ²²⁸Th, which have half-lives of 5.75 and 1.91 years respectively (Indongo and Mathuthu 2023). The RESRAD

Table 6 RESRAD input parameter

Input parameter	Value	References
Activity concentration (Bqg ⁻¹)		
Ra-226	0.034	Current study
Th-232	0.070	
K-40	0.252	
Exposure duration (year)	30	Default
Area of contamination zone (m ²)	1000	Assumed
Contamination zone thickness (m)	2	Default
Contamination zone density (g/cm ⁻³)	1.51 (loam soil)	Yu et al. (2015)
Wind speed (ms ⁻¹)	1.2	Cameroon (1986)
Area ambient temperature (kelvin)	299.15	Kamtchueng et al. (2016)
Precipitation rate (m/year)	1.59	Kamtchueng et al. (2016)
Runoff rate	0.44	Cameroon (1986)
Irrigation rate (m/year)	0.2	Default
Erosion rate	0.01	Default
Total porosity	0.4	Default
Saturated hydraulic conductivity	219 (loam soil)	Yu et al. (2015)
b parameter	5.39 (loam soil)	Yu et al. (2015)
Transport factor (cm ³ g ⁻¹) for loam soil		
Ra-226	1100	
Th-232	18,000	Yu et al. (2015)
K-40	20	
Release high (m)	2	Default
Inhalation rate	8400	Default
Radon emanation rate		
Rn-222	0.23	Current study
Rn-220	0.16 (loam soil)	Yu et al. (2015)
Effective radon diffusion rate (m ² s ⁻¹)	8 × 10 ⁻⁷ (loam soil)	Yu et al. (2015)
Fraction on time spent onsite		
Indoor	0	Assumed for farmer worker
Outdoor	0.2	
Fraction on time spent offsite		
Indoor	0.6	Assumed for framer worker
Outdoor	0.2	
Water drinking rate (L/year)	510	Default
Soil ingestion rate (g/year)	36.5	Default
Fruit, grain, and non-leafy vegetable consumption rate (kg/year)	160	Default

code models the cancer morbidity risk for ²²⁶Ra. The risk increases from 4.59×10^{-4} at $t=0$ years to 4.93×10^{-4} at 58.9 years, before smoothly decreasing to 4.86×10^{-4} at 100 years. This trend is attributed to the contribution of ²¹⁰Pb and ²¹⁰Po, which have half-lives of 22 years and 138 days respectively, due to their respective ingrowth progenies.

Figure 7 displays the assessment of excess cancer risk resulting from various exposure pathways over 100 years. The data indicate that the external exposure pathway to gamma radiation from soil and air is the most significant contributor, followed by the ingestion pathway of plants and meat from the contaminated area. Figure 8 demonstrates that

for ²²⁶Ra, the external exposure pathway from contaminated soil and air was the most significant contributor to gamma radiation exposure, followed by the inhalation of radon gas. According to Fig. 9, the primary contributors to ²³²Th exposure were external gamma from soil and air.

The ingestion of plants and meat from the contaminated area was the primary route of exposure for ⁴⁰K (Fig. 10), followed by external exposure to gamma radiation from the soil and air. Water pathways did not significantly contribute to the exposure.

The risks calculated experimentally and modelled by the RESRAD-OFFSITE code were also compared for

Table 7 Cancer morbidity risk for each radionuclide, and summed from all pathways for 100 years

Time (year)	Ra-226	Th-232	K-40	Total
0	4.59×10^{-4}	8.65×10^{-4}	1.22×10^{-3}	2.78×10^{-3}
1	4.61×10^{-4}	8.82×10^{-4}	1.20×10^{-3}	2.76×10^{-3}
5	4.66×10^{-4}	9.39×10^{-4}	1.14×10^{-3}	2.70×10^{-3}
10	4.72×10^{-4}	49.84×10^{-4}	1.06×10^{-3}	2.62×10^{-3}
30	4.87×10^{-4}	1.04×10^{-3}	8.13×10^{-4}	2.37×10^{-3}
58.9	4.93×10^{-4}	1.04×10^{-3}	5.51×10^{-4}	2.09×10^{-3}
75	4.91×10^{-4}	1.04×10^{-3}	4.44×10^{-4}	1.98×10^{-3}
100	4.86×10^{-4}	1.04×10^{-3}	3.17×10^{-4}	1.85×10^{-3}

The data in bold represent the long-term cancer risk obtained by the Resrad offsite simulation for each radionuclide and the total risk related to Cameroonian expectancy life of 58.9 years

58.9 years, corresponding to the life expectancy of the population living in the study area. The values recorded for the calculated risk of 1.86×10^{-3} and the modelled risk of 2.09×10^{-3} , showed a slight overestimation of the risk obtained by simulation. The ratio between the simulated and experimental values was 1.12. This overestimation modelled risk can be attributed to the contribution of the daughter progeny of the various radionuclides used in the RESRAD code to calculate the risk, whereas the experimental calculation only takes into account the main radionuclides.

Additionally, it could be due to the fact that for certain parameters the default values were used in the simulation instead of the parameters of the study area.

Conclusions

In this study, the estimation of activity concentrations of primordial radionuclides (^{226}Ra , ^{232}Th , and ^{40}K) using gamma-ray spectrometry based on the HPGe detector and the related health risk hazard was determined. The measured average activity concentration of ^{226}Ra , and ^{232}Th recorded herein were above the world average values reported by UNCEAR (2000). The obtained average activity concentration of ^{40}K was below the world average value reported by UNSCEAR (2000), with 14% of soil sample activity concentration above this value.

The registered average values of different radiological parameters were slightly higher than their world average values. However, for each parameter assessed, the recorded whole value is still within the acceptable range compared with other published studies. For the $\text{EDR}_{\text{organ}}$ and hazard indices, the reported value was below the international tolerable limit of $1.0 \text{ mSv}\cdot\text{yr}^{-1}$ and the unity, respectively. Based on this, it appears that the area investigated does not pose an immediate radiological risk to those living

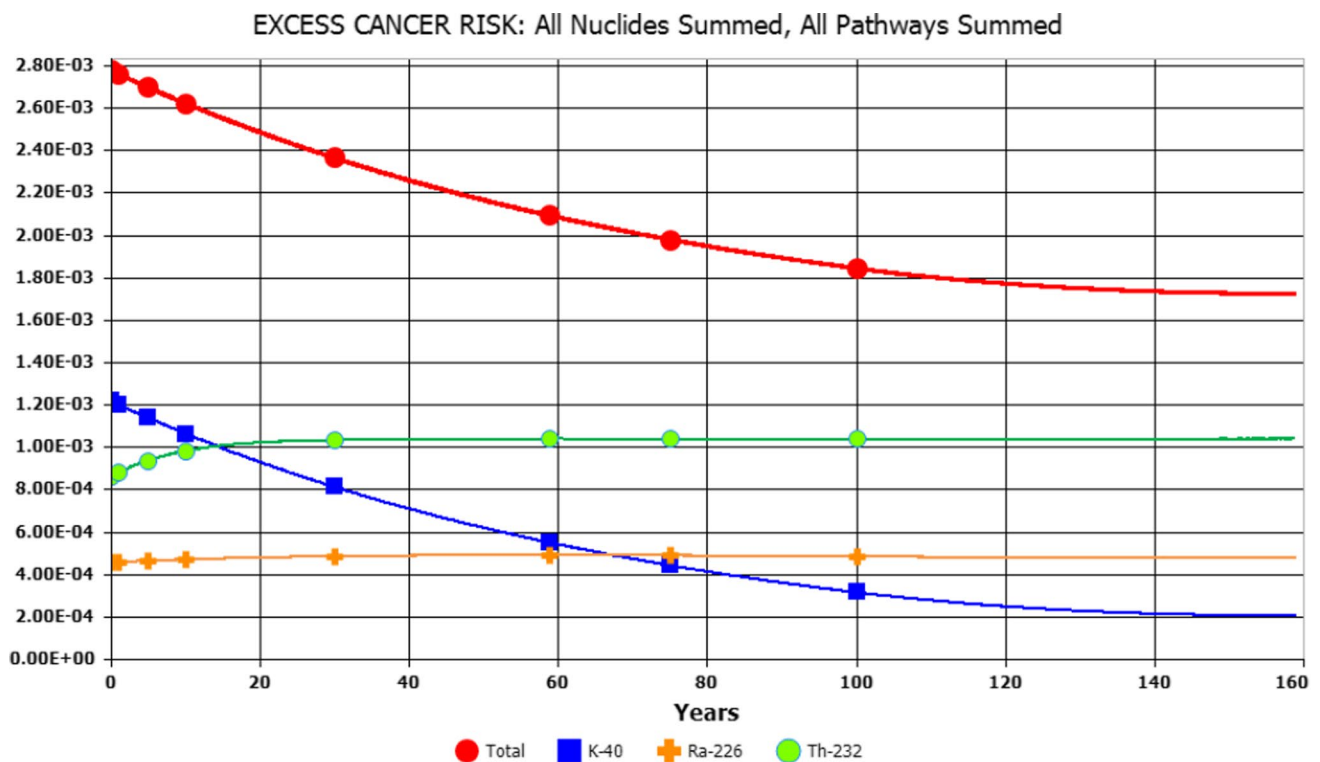


Fig. 6 Excess cancer risk from all radionuclides and all pathways summed during 100 years

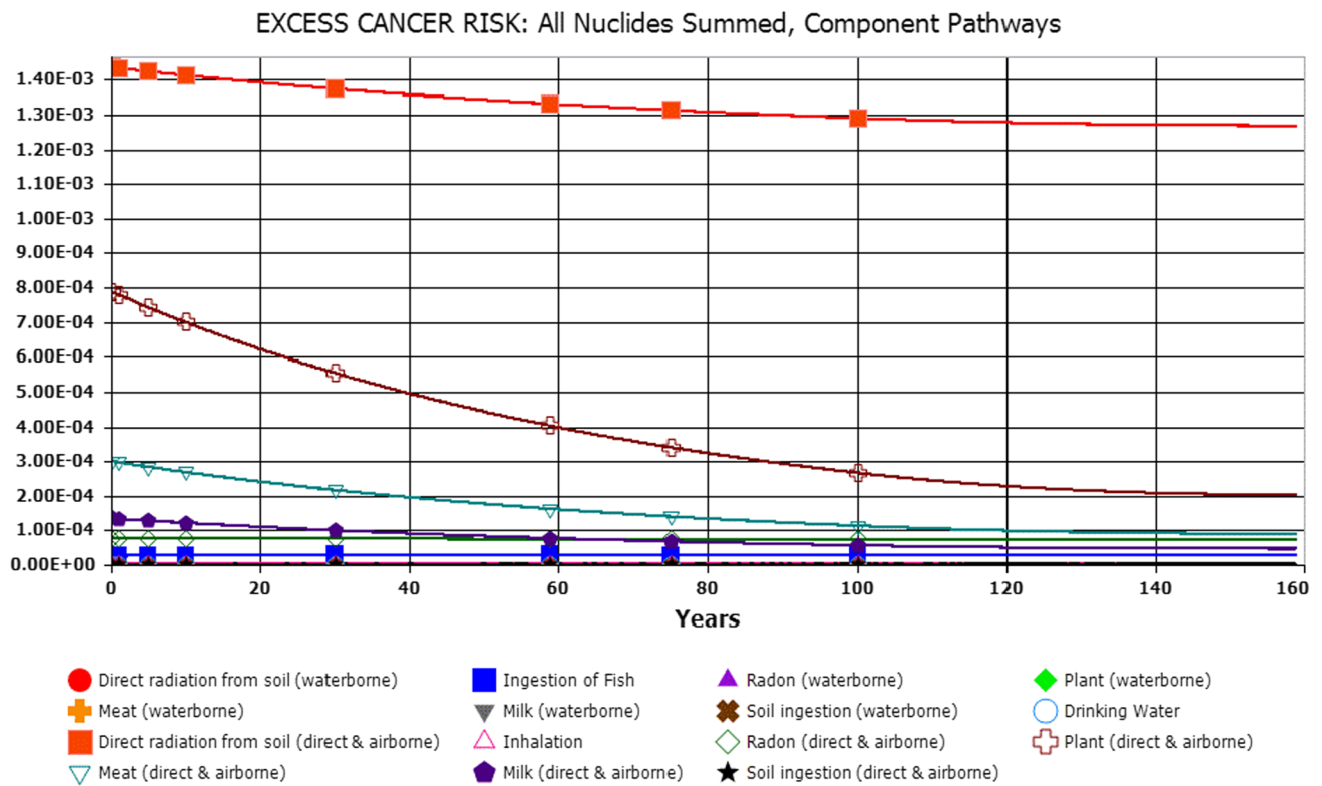


Fig. 7 Cancer morbidity risk from all radionuclides summed, considering all exposure pathways

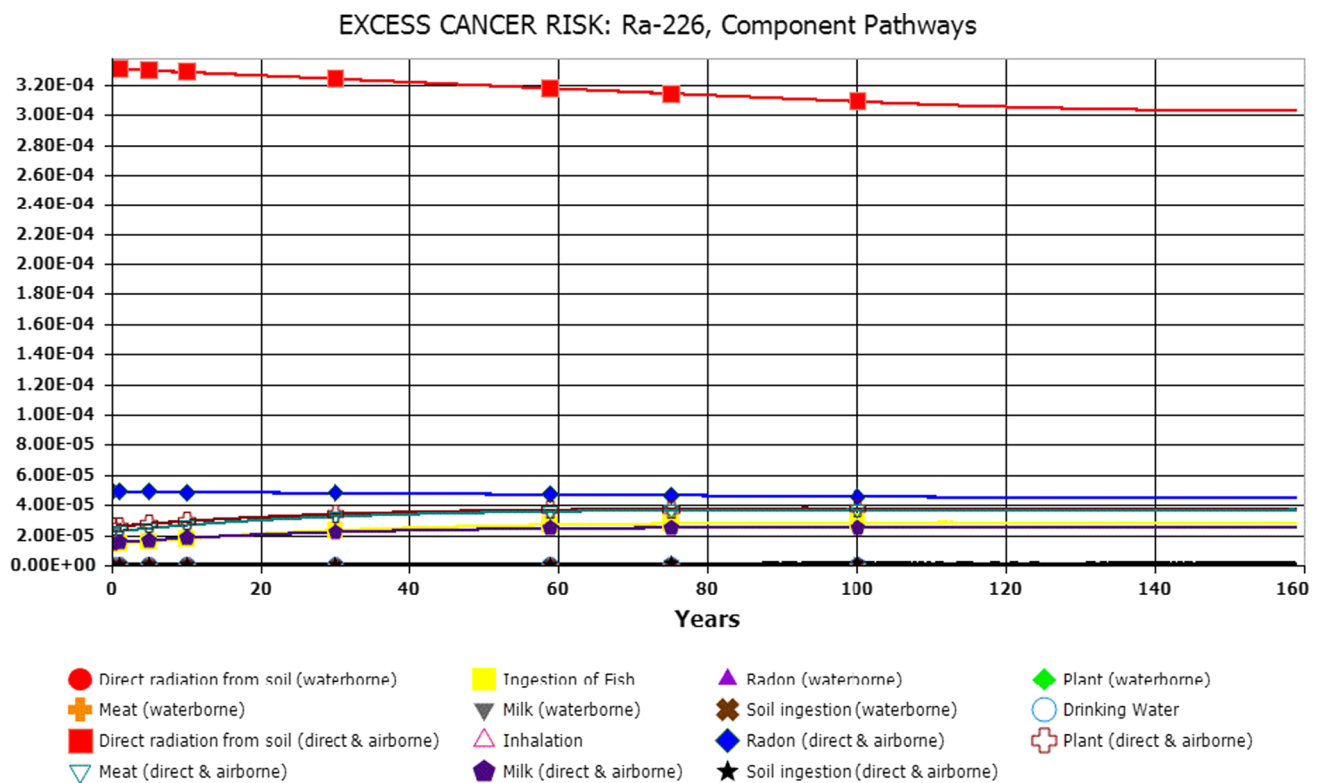


Fig. 8 Excess cancer risk from ²²⁶Ra, considering all exposure routes during 100 years

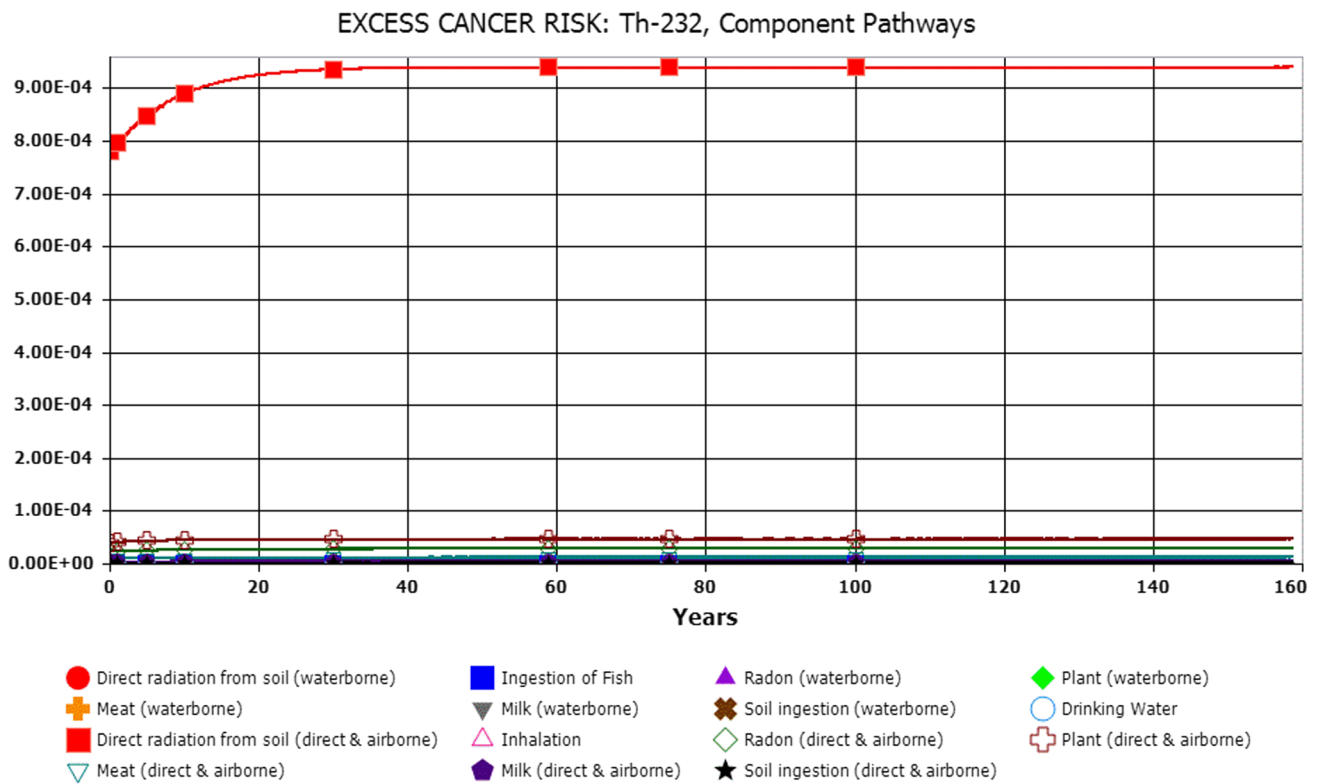


Fig. 9 Excess cancer risk from ²³²Th considering all exposure routes during 100 years

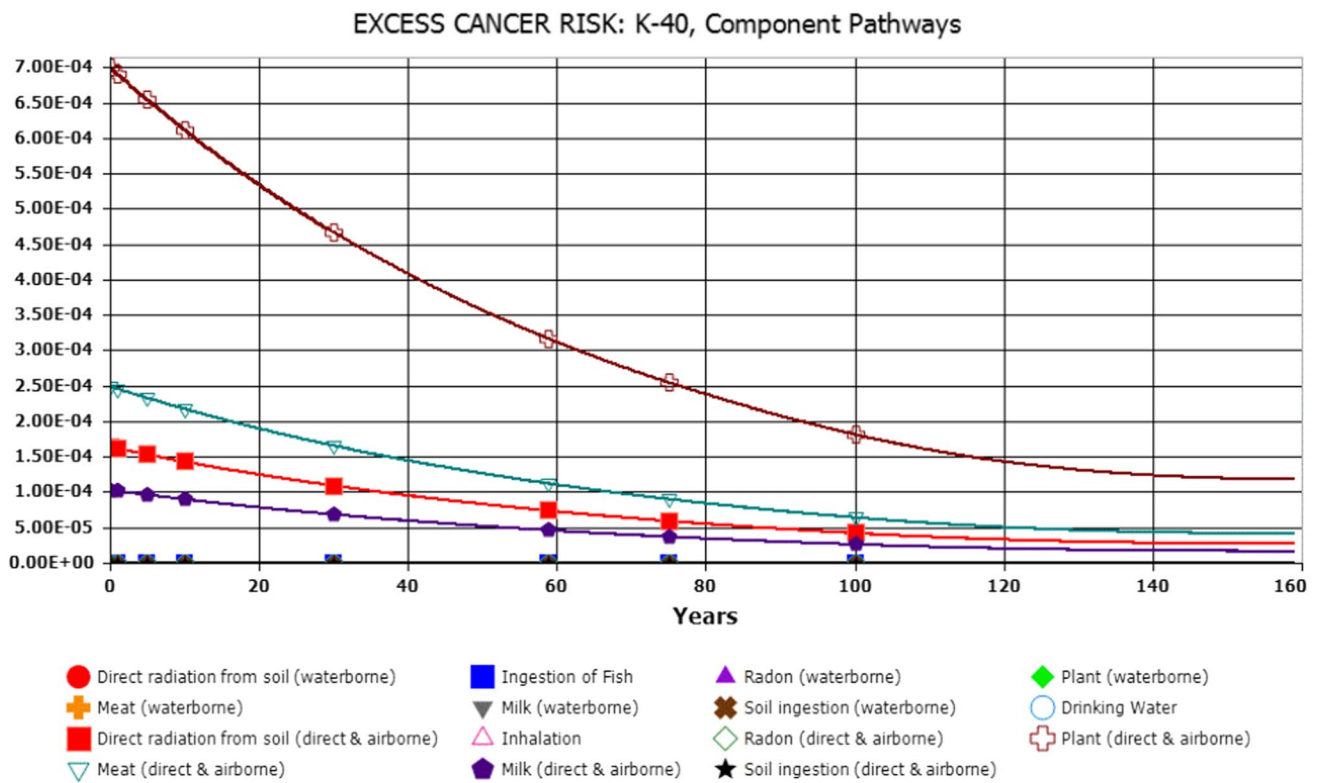


Fig. 10 Excess cancer risk from ⁴⁰K considering all exposure routes during 100 years

in the area or to the general public. However, certain soil samples require special attention if they are to be used as a building material.

Furthermore, the long-term radiological effect was assessed using the RESRAD-OFFSITE computer code. The obtained cancer morbidity risk was found to be above the world limit value of 1.45×10^{-3} (Indongo and Mathuthu 2023) over 100 years. ^{40}K exposure was considered as the main contributor to the excess cancer risk in the first 15 years, followed by ^{232}Th which was the main contributor from 15 years over the 100 years. For ^{232}Th and ^{226}Ra , the external exposure pathways to gamma radiation coming directly from soil and air were the main contributors. The reported radiological data in this study will serve as background reference information on radioactivity distribution in the area and will be helpful for future assessment.

Acknowledgements The authors would like to extend their thanks to the Ghanaian Atomic Energy Commission (GAEC) for the technical support and equipment provided during spectra acquisition and data analysis and most especially for their useful discussions, guidance, and help provided in reviewing the manuscript and for making their facilities available for this research work. We would like to thank the Research Centre for Nuclear Science and Technology, Institute of Geological and Mining Research (IRGM), Cameroon for the technical support and equipment provided during samples preparations. We would also like to thank the ICTP for financial support through the OEA-AF-12 project. Our gratitude goes to the local community around the LM during the sampling campaign for their guidance on the field.

Author contributions Felix Haman: Conceptualization, Methodology, Data collection, analysis, and Writing—original draft preparation & editing; David Kpeglo Okoh: Data collection, analysis, and Writing—review & editing; Daniel Bongue: Conception, Writing—review & editing; Sebastien Joel Guembou Shouop: Conception, design, Methodology, Writing—original draft preparation, and Writing—review & editing; Dorine Flore Tiomene: Data collection and analysis; Dieu Souffit Gondji: Analysis and Writing—review & editing; Maurice Ndongtchueng Moyo: Resources, Project administration, Conception, design, Writing—review & editing.

Funding This work was supported by The Abdus Salam International Centre for Theoretical Physics (ICTP) through the OEA-AF-12 project at Centre for Atomic Molecular Physics and Quantum Optics (CEPAMOQ), Cameroon.

Availability of data and materials All data generated and analysed during this study will be made available upon reasonable request.

Declarations

Conflict of interest The authors have no competing interests to declare that are relevant to the content of this article.

Ethical approval Not applicable.

Ethical approval for animal research This article does not contain any studies on animals performed by any authors.

Ethical responsibilities for authors All authors have read, understood, and have complied as applicable with the statement on “Ethical responsibilities of Authors” as found in the Instructions for Authors.

Consent to participate No human participants were involved in this study.

References

- Abdullahi S, Ismail AF, Samat S (2019) Determination of indoor doses and excess lifetime cancer risks caused by building materials containing natural radionuclides in Malaysia. *Nucl Eng Technol* 51:325–336. <https://doi.org/10.1016/j.net.2018.09.017>
- Alzubaidi G, Hamid FBS, Abdul Rahman I (2016) Assessment of natural radioactivity levels and radiation hazards in agricultural and virgin soil in the State of Kedah North of Malaysia. *Sci World J*. <https://doi.org/10.1155/2016/6178103>
- Avwiri OCP, Tutumeni GO (2016) Measurement of natural radioactivity and evaluation of radiation hazards in soil of Abua/Odual Districts using multivariate statistical approach
- Cameroon (1986) Feasibility report on Baigom Agricultural development project. Annex ; volume 2. https://openjicareport.jica.go.jp/807/807/807_505_10296366.html. Accessed 6 Jun 2023
- Chauhan RP, Chauhan P, Pundir A et al (2014) Estimation of dose contribution from ^{226}Ra , ^{232}Th and ^{40}K radon exhalation rates in soil samples from Shivalik foot hills in India. *Radiat Prot Dosim* 158:79–86. <https://doi.org/10.1093/RPD/NCT190>
- Cui Z, Lu X, Zhang W et al (2022) Investigation of two-phase jet flow from a degassing pipe used for a lake with potential gas-driven eruption. *JVGR* 425:107529. <https://doi.org/10.1016/J.JVOLGEORES.2022.107529>
- Dabayneh KM, Mashal LA, Hasan FI (2008) Radioactivity concentration in soil samples in the southern part of the West Bank, Palestine. *Radiat Prot Dosimetry* 131:265–271. <https://doi.org/10.1093/RPD/NCN161>
- Darwish DAE, Abul-Nasr KTM, El-Khayatt AM (2015) The assessment of natural radioactivity and its associated radiological hazards and dose parameters in granite samples from South Sinai. *Egypt J Radiat Res Appl Sci* 8:17–25. <https://doi.org/10.1016/j.jrras.2014.10.003>
- El-Gamal A, Nasr S, El-Taher A (2007) Study of the spatial distribution of natural radioactivity in the upper Egypt Nile River sediments. *Radiat Meas* 42:457–465. <https://doi.org/10.1016/j.radmeas.2007.02.054>
- Faanu A, Lawluvi H, Kpeglo DO et al (2014) Assessment of natural and anthropogenic radioactivity levels in soils, rocks and water in the vicinity of chirano gold mine in Ghana. *Radiat Prot Dosim* 158:87–99. <https://doi.org/10.1093/rpd/nct197>
- Gondji DS, Monempimb JV, Oumar BM et al (2022) Risk assessment of exposure to natural radiation in soil using RESRAD-ONSITE and RESRAD-BIOTA in the cobalt-nickel bearing areas of Lomié in Eastern Cameroon. *Radiation* 2:177–192. <https://doi.org/10.3390/radiation2020013>
- Guembou Shouop CJ, Ndontchueng Moyo M, Chene G et al (2017) Assessment of natural radioactivity and associated radiation hazards in sand building material used in Douala Littoral Region of Cameroon, using gamma spectrometry. *Environ Earth Sci*. <https://doi.org/10.1007/s12665-017-6474-3>
- Guembou Shouop CJ, Ndontchueng Moyo M, Nguemlem Mekongtso EJ et al (2021) Application of energy dispersive X-ray fluorescence, γ -ray spectrometry and multivariate statistical approach for the classification of soil/sand from Douala—Cameroon. *Radiat Phys Chem*. <https://doi.org/10.1016/j.radphyschem.2021.109589>
- Hartwell JK (1975) Detection limits for : radioanalytical counting techniques, pp 5–48
- Hussain M, Rafique Q, Hussain M et al (2017) Modeling radiation doses for a hypothetical contaminated site using RESRAD-OFFSITE

- Code Faisalabad, Pakistan the nucleus modeling radiation doses for a hypothetical contaminated site using RESRAD-OFFSITE code Faisalabad, Pakistan. *Nucl* 54:33–37
- Idriss H, Salih I, Alaamer AS et al (2016) Environmental-impact assessment of natural radioactivity around a traditional mining area in Al-Ibedia, Sudan. *Arch Environ Contam Toxicol* 70:783–792. <https://doi.org/10.1007/s00244-016-0271-y>
- Indongo V, Mathuthu M (2023) Modelling of radiological health hazards in tailing soils from uranium mines in Erongo Region. *Namibia* 11:1–8
- Issa OT, Chako Tchamabé B et al (2014) Gas emission from diffuse degassing structures (DDS) of the Cameroon volcanic line (CVL): implications for the prevention of CO₂-related hazards. *J Volcanol Geotherm Res* 283:82–93. <https://doi.org/10.1016/j.jvolgeoes.2014.07.001>
- James IU, Moses IF, Akueche EC, Kuwen RD (2020) Assessment of indoor and outdoor radiation levels and human health risk in Sheda Science and Technology Complex and its environ, Abuja Nigeria. *J Appl Sci Environ Manag* 24:13. <https://doi.org/10.4314/jasem.v24i1.2>
- Kamtchueng BT, Fantong WY, Wirmvem MJ et al (2016) Hydrogeochemistry and quality of surface water and groundwater in the vicinity of Lake Monoun, West Cameroon: approach from multivariate statistical analysis and stable isotopic characterization. *Environ Monit Assess*. <https://doi.org/10.1007/s10661-016-5514-x>
- Kayakökü H, Doğru M (2017) Radioactivity analysis of soil samples taken from the western and northern shores of Lake Van, Turkey. *Appl Radiat Isot* 128:231–236. <https://doi.org/10.1016/j.apradiso.2017.07.019>
- Kiprotich Langat W, Ambusso NOWHJ (2014) Gamma ray spectrometric analysis of sedimental deposits at the shores of Lake Nakuru, Kenya. Online
- Kling GW, Evans WC, Tanyileke GZ (2015) The comparative limnology of lakes Nyos and Monoun Cameroon. *Adv Volcanol*. https://doi.org/10.1007/978-3-642-36833-2_18
- Kurnaz A, Turhan A, Hançerlioğulları A et al (2020) Natural radioactivity, radon emanating power and mass exhalation rate of environmental soil samples from Karabük province, Turkey. *Radiochim Acta* 108:573–579. <https://doi.org/10.1515/ract-2019-3188>
- Kusakabe M (2017) Lakes nyos and monoun gas disasters (Cameroon)—limnic eruptions caused by excessive accumulation of magmatic CO₂ in crater lakes. *Geochem Monogr Ser* 1:1–50. <https://doi.org/10.5047/gems.2017.00101.0001>
- Li J, Hu B, Zhao J et al (2017) Evaluation of natural radioactivity in marine sand deposits from offshore China. *Open J Mar Sci* 07:357–378. <https://doi.org/10.4236/ojms.2017.73026>
- Mann N, Kumar A, Kumar S, Chauhan RP (2018) Measurement of radium, thorium, potassium and associated hazard indices from the soil samples collected from Northern India. *Indoor Built Environ* 27:1149–1156. <https://doi.org/10.1177/1420326X17696136>
- Mekongtso Nguelem EJ, Moyo Ndongtchueng M, Motapon O (2016) Determination of ²²⁶Ra, ²³²Th, ⁴⁰K, ²³⁵U and ²³⁸U activity concentration and public dose assessment in soil samples from bauxite core deposits in Western Cameroon. Springerplus. <https://doi.org/10.1186/s40064-016-2895-9>
- Mishra P, Pandey CM, Singh U et al (2019) Descriptive statistics and normality tests for statistical data. *Ann Card Anaesth* 22:67–72. https://doi.org/10.4103/aca.ACA_157_18
- Mottet G (2000) Les Lacs d'origine volcanique (Volcanic Origin Lakes). *Bulletin De L'association De Géographes Français* 4:337–345
- Ndjana Nkoulou III JE, Feutseu Talla S, Bineng GS et al (2018) Natural radioactivity measurements in soil external dose and radiological hazard assessment in the uranium and thorium bearing region of Lolodorf Cameroon. *Radioisotopes* 67:435–446. <https://doi.org/10.3769/radioisotopes.67.435>
- Ndongtchueng MM, Mekongtso Nguelem EJ, Simo A et al (2014) Gamma emitting radionuclides in soils from selected areas in Douala-Bassa zone, littoral region of Cameroon. *ISRN Spectrosc* 2014:1–8. <https://doi.org/10.1155/2014/245125>
- Ngachin M, Garavaglia M, Giovani C et al (2007) Assessment of natural radioactivity and associated radiation hazards in some Cameroonian building materials. *Radiat Meas* 42:61–67. <https://doi.org/10.1016/J.RADMEAS.2006.07.007>
- Ogundele LT, Ayeku PO, Inuyomi SO et al (2020) Assessment of naturally occurring ⁴⁰K, ²³²Th and ²³⁸U and their associated radiological hazard indices in soils used for building in Ondo West Local Government area, Southwestern, Nigeria. *Int J Environ Qual* 37:11–21. <https://doi.org/10.6092/issn.2281-4485/9473>
- Ohba T, Oginuma Y, Saiki K et al (2022) A depression containing CO₂-enriched water at the bottom of Lake Monoun, Cameroon, and implications for the 1984 limnic eruption. *Front Earth Sci* 10:1–15. <https://doi.org/10.3389/feart.2022.766791>
- Penabei S, Bongue D, Maleka P et al (2018) Assessment of natural radioactivity levels and the associated radiological hazards in some building materials from Mayo-Kebbi region, Chad. *Radioprotection* 53:265–278. <https://doi.org/10.1051/radiopro/2018030>
- Penabei S, Bongue D, Eyakifama H et al (2022) Health risk assessment and statistical analysis of natural radioactivity in the uranium exploration area of Zabili Chad. *Int J Environ Anal Chem*. <https://doi.org/10.1080/03067319.2022.2152687>
- Ravisankar R, Vanasundari K, Suganya M et al (2014) Multivariate statistical analysis of radiological data of building materials used in tiruvannamalai, tamilnadu, india. *Appl Radiat Isot* 85:114–127. <https://doi.org/10.1016/j.apradiso.2013.12.005>
- Rouwet D, Christenson B, Tassi F, Vandemeulebrouck J (2015) Volcanic lakes. *Volcan Lakes*. <https://doi.org/10.1007/978-3-642-36833-2>
- Sigurdsson H, Devine JD, Tchua FM et al (1987) Origin of the lethal gas burst from Lake Monoun, Cameroon. *J Volcanol Geotherm Res* 31:1–16. [https://doi.org/10.1016/0377-0273\(87\)90002-3](https://doi.org/10.1016/0377-0273(87)90002-3)
- Sivakumar S, Chandrasekaran A, Ravisankar R et al (2014) Measurement of natural radioactivity and evaluation of radiation hazards in coastal sediments of east coast of Tamilnadu using statistical approach. *J Taibah Univ Sci* 8:375–384. <https://doi.org/10.1016/j.jtusci.2014.03.004>
- Tassi F, Rouwet D (2014) An overview of the structure, hazards, and methods of investigation of nyos-type lakes from the geochemical perspective. *J Limnol* 73:39–54. <https://doi.org/10.4081/jlimnol.2014.836>
- Tiomene DF, Bongue D, Guembou Shouop CJ et al (2023) Environmental impact assessment and statistical analysis of natural radioactivity in the slopes of Mount Cameroon area. *Arab J Geosci* 16:1–15. <https://doi.org/10.1007/s12517-023-11511-0>
- Turhan Ş, Gören E, Uğur FA et al (2018) Study of the radioactivity in environmental soil samples from Eastern Anatolia Region of Turkey. *Radiochim Acta* 106:161–168. <https://doi.org/10.1515/ract-2017-2845>
- UNSCEAR (2000) Sources and effects of ionizing radiation
- Yalcin F, Ilbeyli N, Demirbilek M et al (2020) Estimation of natural radionuclides' concentration of the plutonic rocks in the Sakarya zone, Turkey using multivariate statistical methods. *Symmetry (basel)* 12:1–18. <https://doi.org/10.3390/sym12061048>

- Yu C, Gnanapragasam E, Biber B et al (2009) RESRAD-OFFSITE—a new member of the RESRAD family of codes. *Radioprotection* 44:659–664. <https://doi.org/10.1051/radiopro/20095121>
- Yu C, Kamboj S, Wang C, Cheng J-J (2015) Data collection handbook to support modeling impacts of radioactive material in soil and building structures <https://doi.org/10.2172/1224969>
- Yu C, Gnanapragasam E, Cheng J-J, et al (2020) User's manual for RESRAD-OFFSITE code version 4. 1

Springer Nature or its licensor (e.g. a society or other partner) holds exclusive rights to this article under a publishing agreement with the author(s) or other rightsholder(s); author self-archiving of the accepted manuscript version of this article is solely governed by the terms of such publishing agreement and applicable law.

Publisher's Note Springer Nature remains neutral with regard to jurisdictional claims in published maps and institutional affiliations.